

DFTT 27/02
 CERN-TH/2002-191
 IPPP/02/48
 DCPT/02/96
 SHEP-02/24
 September 2002

Weak Corrections to Three-Jet Production in Electron-Positron Annihilations*

E. Maina

Dipartimento di Fisica Teorica – Università di Torino
Via Pietro Giuria 1, 10125 Torino, Italy
and
Istituto Nazionale di Fisica Nucleare – Sezione di Torino
Via Pietro Giuria 1, 10125 Torino, Italy
E-mail: maina@to.infn.it

S. Moretti

CERN – Theory Division
CH-1211 Geneva 23, Switzerland
and
Institute for Particle Physics Phenomenology – University of Durham
South Road, Durham DH1 3LE, UK
E-mails: stefano.moretti@cern.ch, stefano.moretti@durham.ac.uk

D.A. Ross

Department of Physics and Astronomy – University of Southampton
Highfield, Southampton SO17 1BJ, UK
Email: dar@hep.phys.soton.ac.uk

ABSTRACT: We report on the calculation of the factorisable one-loop weak-interaction corrections to the initial and final states for three-jet observables in electron-positron annihilations. We show that whereas such corrections are negligibly small at LEP energies they are significantly enhanced at a future Linear Collider, where we argue that they may be similar in size to the two-loop QCD effects. The calculation has been performed using helicity amplitudes so that it can be applied to the case of polarised beams. The effects of beam polarisation can be extracted from an analysis of the angular distributions of the jets relative to the incident electron/positron directions.

KEYWORDS: QCD processes, Electroweak effects, Loop calculations, Lepton colliders.

*Work supported in part by the U.K. Particle Physics and Astronomy Research Council (PPARC), by the

Contents

1. Electroweak corrections at high energies	1
2. One-loop weak effects in three-jets events at leptonic colliders	3
3. Calculation	3
4. Numerical results	7
5. Conclusions	12

1. Electroweak corrections at high energies

Strong (QCD) and Electroweak (EW) interactions are two fundamental forces of Nature, the latter in turn unifying weak and electromagnetic (EM) interactions. Together they constitute the Standard Model (SM) of particle physics. A clear hierarchy exists between the strengths of the two interactions at the energy scales probed by past and present high energy particle accelerators (e.g., LEP, SLC, HERA, RHIC and Tevatron): QCD forces are stronger than EW ones. This is quantitatively manifest if one recalls that the value of the QCD coupling ‘constant’, α_S , measured at these machines is much larger than the EW one, α_{EW} , typically, by an order of magnitude.

The above-mentioned particle accelerators have been operating at the so-called ‘EW scale’, $\mathcal{O}(M_{EW})$, around the mass of the EW gauge bosons, $M_{EW} \sim M_W \sim M_Z$. (Recall that the energy at which partons are scattered in hadronic collisions is only a fraction the actual beam energy.) However, the future generation of machines, such as the approved proton-proton Large Hadron Collider (LHC) and the proposed electron-positron Linear Collider (LC) [1], will enter the multi-TeV energy regime. The centre-of-mass (CM) energy of the LHC will in fact be 14 TeV whereas current designs of LCs consider values up to 3 TeV or so.

At such high energy scales, this hierarchy between QCD and EW interactions may no longer be respected. The reason is twofold. On the one hand, while both coupling constants become smaller with increasing energy, the evolution (or ‘running’) with energy of α_S is faster than for α_{EW} . On the other hand, weak corrections to production cross-sections are enhanced by double logarithmic factors which, unlike in QCD, do not cancel for ‘infrared-safe’ observables. For example, at one-loop level, in the case of the inclusive cross-section of e^+e^- into hadrons, the QCD corrections are of $\mathcal{O}(\frac{\alpha_S}{\pi})$, whereas the EW ones are of

European Union (EU) under contract HPRN-CT-2000-00149 and by the Italian Ministero dell’Istruzione, dell’Università e della Ricerca (MIUR) under contract 2001023713-006.

$\mathcal{O}(\frac{\alpha_{\text{EW}}}{4\pi} \log^2 \frac{s}{M_W^2})$, where s is the collider CM energy squared [2] – [4]. At $\sqrt{s} = 1.5$ TeV, the former are identical to the latter, of order 9% or so. The two aspects may combine, giving rise to some manifestations (both at the LHC and a LC) of the two forces which are of similar size.

The origin of these ‘double logs’ is understood. It is due to a lack of cancellation of infrared (both soft and collinear) virtual and real emission in higher order contributions. This is in turn a consequence of the violation of the Bloch-Nordsieck theorem in non-Abelian theories [5]¹. The problem is in principle present also in QCD. In practice, however, it has no observable consequences, because of the final averaging of the colour degrees of freedom of partons, forced by their confinement into colourless hadrons. This does not occur in the EW case, where, e.g., the initial state has a non-Abelian charge, dictated by the given collider beam configuration, such as in e^+e^- collisions. Needless to say, the same argument also holds for an initial quark doublet in proton-proton scatterings. These logarithmic corrections (unless the EW process is mass-suppressed) are universal (i.e., process independent) and are finite (unlike in QCD), as the masses of the EW gauge bosons provide a physical cut-off for W - and Z -emission. Hence, for typical experimental resolutions, softly and collinearly emitted weak bosons need not be included in the production cross-section and one can restrict oneself to the calculation of weak effects originating from virtual corrections and affecting a purely hadronic final state. Besides, these contributions can be isolated in a gauge-invariant manner from purely EM effects [4], [8] – [12], which may or may not be included in the calculation, depending on the observable being studied.

In view of this, it becomes of crucial importance to assess the quantitative relevance of such weak corrections affecting, in particular, key QCD processes studied at present at future colliders [13]. (See Refs. [8] – [33] for a collection of papers dealing with resummed, one- and two-loop EW corrections to various high energy processes.) It is the aim of our paper to report on the computation of the one-loop weak effects entering three-jet production in electron-positron annihilation via the subprocess $e^+e^- \rightarrow \gamma^*, Z^{(*)} \rightarrow \bar{q}qg^2$, when the higher order effects arise only from initial or final state interactions. These represent the so-called ‘factorisable’ corrections, i.e., those involving loops not connecting the initial leptons to the final quarks. The remainder, ‘non-factorisable’ corrections, while being negligible at $\sqrt{s} = M_Z$ (where the width of the Z resonance provides a natural cut-off for off-shellness effects), are expected to play a quantitatively relevant role as \sqrt{s} grows larger. The latter will however be the subject of a future publication. Here, we will focus our attention on the former at typical LEP1/SLC, LEP2 and LC energies, with and without the option of beam polarisation. While one-loop weak effects are expected to appear at the percent level at LEP1/SLC, sizable logarithmic enhancement or suppression should

¹Recently, it has been found that Bloch-Nordsieck violation can also occur in spontaneously broken Abelian gauge theories, if the incoming particles are mass eigenstates that do not coincide with gauge eigenstates [6]. In the SM this is particularly relevant for incoming longitudinal gauge bosons or Higgs scalars [7].

²See Ref. [34] for the corresponding weak corrections to the Born process $e^+e^- \rightarrow \bar{q}q$ and Ref. [35] for the $\sim n_f$ component of those to $e^+e^- \rightarrow \bar{q}qgg$ (where n_f represents the number of light flavours). For two-loop results on the former, see [22].

already be visible at LEP2, while becoming comparable to the one-loop QCD corrections at LCs.

On the subject of higher order QCD effects, it should be mentioned that a great deal of effort has recently been devoted to evaluate two-loop contributions to the three-jet process³ (albeit, only at the amplitude level so far, as there are no numerical results available yet). However, we will argue in our study that one-loop weak effects are equally important, particularly as one increases the CM energy of the collider.

2. One-loop weak effects in three-jets events at leptonic colliders

In the case of e^+e^- annihilations, the most important QCD quantity to be extracted from multi-jet events is precisely α_s . The confrontation of the measured value of the strong coupling constant with that predicted by the theory through the renormalisation group evolution is an important test of the SM or else an indication of new physics, whose typical mass scale is larger than the collider energy, but which can manifest itself through virtual effects. Jet-shape observables, which offer a handle on non-perturbative QCD effects via large power corrections, would be affected as well.

A further aspect that should be recalled is that weak corrections naturally introduce parity-violating effects in jet observables, detectable through asymmetries in the cross-section, which are often regarded as an indication of physics beyond the SM. These effects are further enhanced if polarisation of the incoming beams is exploited. Although at past and present polarised colliders (such as SLC and RHIC) parity-violating weak effects are threshold suppressed because the machines operate close to the EW scale, this will no longer be true at future accelerators. While there exists a realistic possibility of exploiting beam polarisation at the LHC, this option is one of the strengths of the LC projects. Comparison of theoretical predictions involving parity-violation with future experimental data is regarded as another powerful tool for confirming or disproving the existence of some beyond the SM scenarios, such as those involving right-handed weak currents and/or new massive gauge bosons.

The plan of the rest of the paper is as follows. In the next Section, we describe the calculation. Then, in Sect. 4, we present some numerical results. We conclude in Sect. 5.

3. Calculation

Since we are considering weak corrections that can be identified via their induced parity-violating effects and since we wish to apply our results to the case of polarised electron and/or positron beams, it is convenient to work in terms of helicity matrix elements (MEs). Thus, we define the helicity amplitudes $\mathcal{A}_{\lambda_1, \lambda_2, \sigma}^{(G)}$ for an off-shell gauge boson of type G (hereafter, a photon γ or a Z -boson) of helicity λ_1 decaying into a gluon with helicity λ_2 , a massless quark with helicity σ and a massless antiquark with opposite helicity⁴. Since the

³The one-loop QCD results have been known for some time [36].

⁴Note that all interactions considered here preserve the helicity along the fermion line, including those in which Goldstone bosons appear inside the loop, since these either occur in pairs or involve a mass insertion on the fermion line.

gauge boson is off-shell, the helicity λ_1 can take the values $+1, 0, -1$, where 0 indicates the longitudinal polarisation, whereas λ_2 and σ can only be equal to ± 1 .

The general form of these amplitudes may be written as

$$\mathcal{A}_{\lambda_1, \lambda_2, \sigma}^{(G)} = \bar{u}(p_2) \Gamma \frac{(1 + \sigma \gamma^5)}{2} v(p_1), \quad (3.1)$$

where p_1 and p_2 are the momenta of the outgoing antiquark and quark respectively and Γ stands for a sum of strings of Dirac γ -matrices with coefficients, which, beyond tree level, involve integrals over loop momenta. Since the helicity σ of the fermions is conserved the strings must contain an odd number of γ -matrices. Repeated use of the Chrystoffel identities⁵ means that Γ can always be expressed in the form

$$\Gamma = C_1 \gamma \cdot p_1 + C_2 \gamma \cdot p_2 + C_3 \gamma \cdot p_3 + C_4 \sqrt{Q^2} \gamma \cdot n, \quad (3.2)$$

where p_3 is the momentum of the outgoing gluon, $Q^2 = (p_1 + p_2 + p_3)^2$ is the square momentum of the gauge boson, and n is a unit space-like vector normal to the jet plane. The coefficient functions C_i depend on the helicities $\lambda_1, \lambda_2, \sigma$ as well as the energy fractions x_1 and x_2 of the antiquark and quark in the final state and on all the couplings and masses of particles that enter into the relevant perturbative contribution to the amplitude.

For massless fermions the MEs of the first two terms of eq. (3.2) vanish, and we are left with

$$\begin{aligned} \mathcal{A}_{\lambda_1, \lambda_2, \sigma}^{(G)} &= C_3 \bar{u}(p_2) \gamma \cdot p_3 \frac{(1 + \sigma \gamma^5)}{2} v(p_1) + C_4 \sqrt{Q^2} \bar{u}(p_2) \gamma \cdot n \frac{(1 + \sigma \gamma^5)}{2} v(p_1), \\ &= C_3 Q^2 \sqrt{(1 - x_1)(1 - x_2)} - i \sigma C_4 Q^2 \sqrt{x_1 + x_2 - 1}. \end{aligned} \quad (3.3)$$

The relevant coefficient functions C_3 and C_4 are scalar quantities and can be projected on a graph-by-graph basis using the projections

$$C_3 = \text{Tr} \left(\Gamma \gamma \cdot v \frac{(1 + \sigma \gamma^5)}{2} \right), \quad (3.4)$$

where v is the vector

$$v = \frac{(1 - x_2)p_1 + (1 - x_1)p_2 - (x_1 + x_2 - 1)p_3}{2Q^2(1 - x_1)(1 - x_2)},$$

and

$$C_4 = -\frac{1}{2\sqrt{Q^2}} \text{Tr} \left(\Gamma \gamma \cdot n \frac{(1 + \sigma \gamma^5)}{2} \right). \quad (3.5)$$

⁵These identities are only valid in four dimensions. In our case, where we do not have infrared (i.e., soft and collinear) divergences, it is a simple matter to isolate the ultraviolet divergent contributions, which are proportional to the tree-level MEs, and handle them separately. However, in d dimensions one needs to account for the fact that there are $2^{d/4}$ helicity states for the fermions and $(d - 2)$ for the gauge bosons. The method described here will not correctly trap terms proportional to $(d - 4)$ in coefficients of divergent integrals. It is probably for this reason that the formalism of Ref. [65] is considerably more cumbersome than that presented here.

At tree level the helicity amplitudes are only functions of x_1 , x_2 , the EW couplings $g_j^{(G)}$ of the (anti)quark of type j (proportional to $g_W \equiv \sqrt{4\pi\alpha_{EW}}$, with $\alpha_{EW} = \alpha_{EM}/\sin^2\theta_W$, and carrying information on both helicity and flavour of the latter) to the relevant gauge boson and the QCD coupling $g_S \equiv \sqrt{4\pi\alpha_S}$. Specifically, in case of massless (anti)quarks (i.e., $m_q = 0$), we have (here, τ^a represents a colour matrix):

$$\begin{aligned}\mathcal{A}_{1,1,1}^{(G)} &= \mathcal{A}_{-1,-1,-1}^{(G)} = -2ig_j^{(G)} g_S \tau^a \frac{x_1}{\sqrt{(1-x_1)(1-x_2)}}, \\ \mathcal{A}_{1,1,-1}^{(G)} &= \mathcal{A}_{-1,-1,1}^{(G)} = -2ig_j^{(G)} g_S \tau^a \frac{\sqrt{(1-x_1)(1-x_2)}}{x_1}, \\ \mathcal{A}_{0,-1,1}^{(G)} &= \mathcal{A}_{0,1,-1}^{(G)} = -2\sqrt{2}ig_j^{(G)} g_S \tau^a \sqrt{\frac{(1-x_1-x_2)}{x_1}},\end{aligned}\tag{3.6}$$

with all others being zero. These zero values do not, in general, remain such in the presence of weak corrections and this can lead to a relative enhancement of the latter, in comparison to QCD effects at the same order.

At one-loop level such helicity amplitudes acquire higher order corrections from the self-energy insertions on the fermions and gauge bosons shown in Fig. 1, from the vertex corrections shown in Fig. 2 and from the box diagrams shown in Fig. 3. As we have neglected here the masses of the final-state quarks, such higher order corrections depend on the ratio Q^2/M_W^2 , where Q^2 is the square momentum of the gauge boson, as well as the EM coupling constant α_{EM} and the weak mixing angle $s_W \equiv \sin\theta_W$ (with $\alpha_{EW} = \alpha_{EM}/s_W^2$). Furthermore, in the case where the final state fermions are b -quarks, the loops involving the exchange of a W -boson lead to effects of virtual t -quarks, so that the corrections also depend on the ratio m_t^2/M_W^2 . (It is only in this case that the graphs involving the exchange of the Goldstone bosons associated with the W -boson graphs are relevant.)

The self-energy and vertex correction graphs contain ultraviolet divergences. These have been subtracted using the ‘modified’ Minimal Subtraction (\overline{MS}) scheme at the scale $\mu = M_Z$. Thus the couplings are taken to be those relevant for such a subtraction: e.g., the EM coupling, α_{EM} , has been taken to be 1/128 at the above subtraction point. The one exception to this renormalisation scheme has been the case of the self-energy insertions on external fermion lines, which have been subtracted on mass-shell, so that the external fermion fields create or destroy particle states with the correct normalisation.

All these graphs are infrared and collinear convergent so that they may be expressed in terms of Passarino-Veltman [37] functions which are then evaluated numerically. The expressions for each of these diagrams have been calculated using FORM [38] and checked by an independent program based on FeynCalc [39]. For the numerical evaluation of the scalar integrals we have relied on FF [40]. A further check on our results has been carried out by setting the polarisation vector of the photon proportional to its momentum and verifying that in that case the sum of all one-loop diagrams vanishes, as required by gauge invariance. The full expressions for the contributions from these graphs are too lengthy to be reproduced here.

In terms of the helicity MEs we define the following ‘spin-matrix’ tensors, only de-

pending on the polarisation state of the off-shell gauge boson,

$$\mathcal{T}_{\lambda\lambda'}^{(GG')} = \sum_{\lambda_2, \sigma} \mathcal{A}_{\lambda, \lambda_2, \sigma}^{(G)} \left(\mathcal{A}_{\lambda', \lambda_2, \sigma}^{(G')} \right)^\dagger, \quad (3.7)$$

where the (anti)quark and gluon helicities have been summed over. These tensor elements are real at tree level, but in general acquire an imaginary part at one loop arising from the cuts of the loop integrations above the threshold for the production of the internal particles.

Finally, we define the customary nine form-factors, F_1, \dots, F_9 , describing the differential structure of a three-jet final state in terms of the above spin-matrix tensors, as follows:

$$F_i = \frac{\alpha_{\text{EM}}}{512\pi^3} \left[\frac{\left(\eta_A^{L(R)} \right)^2}{Q^2} f_i^{AA} + \frac{(1 - \lambda_e - 4s_W^2)}{4s_W c_W} \frac{\left(\eta_A^{L(R)} \eta_Z^{L(R)} \right)}{\Re\{Q^2 - M_Z^2 + i\Gamma_Z M_Z\}} (f_i^{AZ} + f_i^{ZA}) \right. \\ \left. + \left(\frac{1 - \lambda_e - 4s_W^2}{4s_W c_W} \right)^2 \frac{Q^2 \left(\eta_Z^{L(R)} \right)^2}{(\Re\{Q^2 - M_Z^2 + i\Gamma_Z M_Z\})^2} f_i^{ZZ} \right] \quad (i = 1, \dots, 9), \quad (3.8)$$

where

$$\begin{aligned} f_1^{GG'} &= \left(\mathcal{T}_{1,1}^{GG'} + \mathcal{T}_{0,0}^{GG'} + \mathcal{T}_{-1,-1}^{GG'} \right), \\ f_2^{GG'} &= \mathcal{T}_{0,0}^{GG'}, \\ f_3^{GG'} &= -2 \Re \left(\mathcal{T}_{1,1}^{GG'} - \mathcal{T}_{-1,-1}^{GG'} \right), \\ f_4^{GG'} &= -\sqrt{2} \Re \left(\mathcal{T}_{1,0}^{GG'} + \mathcal{T}_{-1,0}^{GG'} \right), \\ f_5^{GG'} &= -2 \Re \mathcal{T}_{1,-1}^{GG'}, \\ f_6^{GG'} &= 2\sqrt{2} \Re \left(\mathcal{T}_{1,0}^{GG'} - \mathcal{T}_{-1,0}^{GG'} \right), \\ f_7^{GG'} &= \sqrt{2} \Im \left(\mathcal{T}_{0,1}^{GG'} - \mathcal{T}_{0,-1}^{GG'} \right), \\ f_8^{GG'} &= 2 \Im \mathcal{T}_{1,-1}^{GG'}, \\ f_9^{GG'} &= -2\sqrt{2} \Im \left(\mathcal{T}_{0,1}^{GG'} + \mathcal{T}_{0,-1}^{GG'} \right), \end{aligned} \quad (3.9)$$

with $\eta_G^{L(R)}$ the weak correction factor to the coupling of the left(right)-handed electron to the gauge boson G and λ_e the helicity of the incoming electron beam (assumed always to be of opposite helicity to the incoming positron beam).

Up to an overall constant, these form-factors are the same as those introduced, e.g., in Refs. [41, 42]. The last three (F_7, \dots, F_9) can arise for the first time at the one-loop level, since they are proportional to the imaginary parts of the spin-matrix. Besides, F_3 , F_6 and F_7 vanish in the parity-conserving limit and can therefore be used as probes of weak interaction contributions to three-jet production. (Moreover, F_3 and F_6 would be exactly zero at tree level if the leading order process were only mediated by virtual photons.)

These form-factors further generate the double differential cross-section for three-jet production in terms of some event shape variable, S , which is in turn related to x_1, x_2 by some function, s , i.e., $S = s(x_1, x_2)$, and of the polar and azimuthal angles, α, β , between, e.g., the incoming electron beam and the antiquark jet, by⁶

$$\begin{aligned} \frac{d^3\sigma}{dS d\cos\alpha d\beta} = & \int dx_1 dx_2 \delta(S - s(x_1, x_2)) [(2 - \sin^2\alpha) F_1 + (1 - 3\cos^2\alpha) F_2 \\ & + \lambda_e \cos\alpha F_3 + \sin 2\alpha \cos\beta F_4 + \sin^2\alpha \cos 2\beta F_5 + \lambda_e \sin\alpha \cos\beta F_6 \\ & + \sin 2\alpha \sin\beta F_7 + \sin^2\alpha \sin 2\beta F_8 + \lambda_e \sin\alpha \sin\beta F_9]. \end{aligned} \quad (3.10)$$

Note that upon integrating over the antiquark jet angle relative to the electron beam, only the form-factor F_1 survives.

In general, it is not possible to distinguish between quark, antiquark and gluon jets, although the above expression can easily be adapted such that the angles α, β refer to the leading jet. However, (anti)quark jets can be recognised when they originate from primary b -(anti)quarks, thanks to rather efficient flavour tagging techniques (such as μ -vertex devices). We will therefore consider the numerical results for such a case separately.

4. Numerical results

The processes considered here are the following:

$$e^+e^- \rightarrow \gamma^*, Z^{(*)} \rightarrow \bar{q}qg \quad (\text{all flavours}), \quad (4.1)$$

when no assumption is made on the flavour content of the final state, so that a summation will be performed over $q = d, u, c, s, b$ -quarks, and

$$e^+e^- \rightarrow \gamma^*, Z^{(*)} \rightarrow \bar{b}bg, \quad (4.2)$$

limited to the case of bottom quarks only in the final state. As already intimated, all quarks in the final state of (4.1)–(4.2) are taken as massless⁷. In contrast, the top quark entering the loops in both reactions has been assumed to have the mass $m_t = 175$ GeV. The Z mass used was $M_Z = 91.19$ GeV and was related to the W -mass, M_W , via the SM formula $M_W = M_Z \cos\theta_W$, where $\sin^2\theta_W = 0.232$. (Corresponding widths were $\Gamma_Z = 2.5$ GeV and $\Gamma_W = 2.08$ GeV.) For α_S we have used the two-loop expression for $\Lambda_{\overline{\text{MS}}}^{(n_f=4)} = 200$ MeV throughout (yielding, $\alpha_S(M_Z) = 0.11$).

We will be studying processes (4.1)–(4.2) at typical LEP1/SLC ($\sqrt{s} = M_Z$), LEP2 ($\sqrt{s} = 130 - 210$ GeV) and LC ($\sqrt{s} = 350$ GeV – 3 TeV) CM energies. We systematically neglect higher order effects from EM radiation, including those due to Initial State Radiation (ISR) or beamstrahlung. In fact, although these are known to be non-negligible

⁶A qualitative difference between the expressions of the form-factors, F_i ($i = 1, \dots, 9$), used here and those of Refs. [41, 42] is that we do not include the sign of the axial vector coupling of the electron to the exchanged gauge boson in our definitions. In this way the difference between the differential cross-sections for left- and right-handed polarised electron beams is manifest in eq. (3.10).

⁷Mass effects in $e^+e^- \rightarrow \gamma^*, Z^{(*)} \rightarrow \bar{b}bg$ have been studied in [43] and [44].

(especially at LC energies), we expect them to have a similar effect on both the tree-level and one-loop descriptions, hence being irrelevant for our purpose. In this context, we should like to elaborate further on the purely EM corrections to the final state of processes (4.1)–(4.2). Those to the form-factor F_1 have already been calculated, since they can be extracted from the Abelian part of the NLO-QCD corrections (see [36]) by replacing C_F by unity and α_S by α_{EM} . As was pointed out in Ref. [45], these corrections are dominated by a term $\sim \alpha_{\text{EM}}\pi/2$ multiplying the tree-level cross-section. This contribution is $\sim 1\%$ and is independent of the jet event shape. A further correction, associated with the Sudakov form-factor, acts in the negative direction and is subdominant away from the two-jet region (i.e., up to values of ~ 0.95 for the Thrust, see below for its definition). There is no reason to believe that these EM corrections would be enhanced for other form-factors. Furthermore, unlike the weak contributions, final state EM effects are energy independent. Therefore, while we expect the EM and weak corrections to be comparable at LEP1 energies, where the mentioned $\log^2(s/M_W^2)$ enhancement is negligible and where the $1/\sin\theta_W$ factor entering the weak couplings may well compensate for the M_W - and M_Z -driven mass suppression in the propagators of the weak loops, weak effects should gradually take over the purely EM ones as the CM energy grows much larger than M_W .

It is common in the specialised literature to define the n -jet fraction $R_n(y)$ as

$$R_n(y) = \frac{\sigma_n(y)}{\sigma_0}, \quad (4.3)$$

where y is a suitable variable quantifying the space-time separation among hadronic objects and with σ_0 identifying the (energy-dependent) Born cross-section for $e^+e^- \rightarrow \bar{q}q$.

For the choice $\mu = \sqrt{s}$ of the renormalisation scale, one can conveniently write the three-jet fraction in the following form:

$$R_3(y) = \left(\frac{\alpha_S}{2\pi}\right) A(y) + \left(\frac{\alpha_S}{2\pi}\right)^2 B(y) + \dots, \quad (4.4)$$

where the coupling constant α_S and the functions $A(y)$ and $B(y)$ are defined in the $\overline{\text{MS}}$ scheme. An experimental fit of the $R_n(y)$ jet fractions to the corresponding theoretical prediction is a powerful way of determining α_S from multi-jet rates.

Through order $\mathcal{O}(\alpha_S)$ processes (4.1)–(4.2) are the leading order (LO) perturbative contributions to the corresponding three-jet cross-section⁸, as defined via eqs. (4.3)–(4.4). The LO terms, however, receive higher order corrections from both QCD and EW interactions and we are concerned here with the next-to-leading order (NLO) ones only. Whereas at LO all the contributions to the three-jet cross-section come from the tree-level parton process $e^+e^- \rightarrow \bar{q}qg$ (which contributes to the $A(y)$ function above), at NLO the QCD contributions to the three-jet rate (hereafter, denoted by NLO-QCD) are due to two sources. First, the real emission diagrams for the processes $e^+e^- \rightarrow q\bar{q}gg$ and $e^+e^- \rightarrow q\bar{q}Q\bar{Q}$, in which one of the partons is ‘unresolved’. This can happen when one has either two collinear partons within one jet or one soft parton outside the jet. Both these contributions are (in general, positively) divergent. Thanks to the Bloch-Nordsieck [46] and

⁸Hereafter, perturbative contributions are refereed to relatively to the $\mathcal{O}(\alpha_{\text{EM}}^2)$ two-jet rate.

Kinoshita-Lee-Nauenberg [47] theorems, these collinear and soft singularities are cancelled at the same order in α_S by the divergent contributions (generally negative) provided by the second source, namely, the virtual loop graphs. Therefore, after renormalising the coupling constant α_S , a finite three-jet cross-section is obtained and the function $B(y)$ accounts for the above-mentioned three- and four-parton QCD contributions⁹. While the EM component of the EW corrections may be treated on the same footing as the QCD one (with the additional photon playing the role of a second gluon), the weak corrections of interest (hereafter, labelled as NLO-W) only contribute to three-parton final states. Hence, in order to account for the latter, it will suffice to make the replacement

$$A(y) \rightarrow A(y) + A_W(y) \quad (4.5)$$

in eq. (4.4).

The decision as to whether two hadronic objects are unresolved or otherwise is usually taken through the application onto the hadronic final state of a so-called ‘jet clustering algorithm’, wherein the number of *clusters*¹⁰ is reduced one at a time by combining the two most (in some sense) nearby ones. The joining procedure is stopped by testing against some criterion and the final clusters are called jets.

As jet clustering schemes¹¹, we have used a selection of the ‘binary’ ones, in which only two objects are clustered together at any step. Given two clusters labelled as i and j , the measure of their ‘distance’ is normally denoted by y_{ij} and the minimal separation allowed by y_{cut} . The algorithms are the following: the JADE (J) one [49], which uses as a measure of separation the quantity

$$y_{ij}^J = \frac{2E_i E_j (1 - \cos \theta_{ij})}{s}; \quad (4.6)$$

the Durham (D) [50] and the Cambridge (C) [51] ones, both using¹²

$$y_{ij}^D \equiv y_{ij}^C = \frac{2 \min(E_i^2, E_j^2) (1 - \cos \theta_{ij})}{s}; \quad (4.7)$$

the Geneva (G) one [53], for which one has

$$y_{ij}^G = \frac{8 E_i E_j (1 - \cos \theta_{ij})}{9 (E_i + E_j)^2}. \quad (4.8)$$

In eqs. (4.6)–(4.8), E_i and E_j are the energies and θ_{ij} the angular separation of any pair ij of clusters in the final state. The choice of these particular schemes has a simple

⁹In order to calculate these, we make use here of a program based on Ref. [48].

¹⁰Here and in the following, the word ‘cluster’ refers to hadrons or calorimeter cells in the real experimental case, to partons in the theoretical perturbative calculations and also to intermediate jets during the clustering procedure.

¹¹We acknowledge here the well admitted abuse of referring to the various jet ‘finders’ both as algorithms and as schemes, since the last term was originally intended to identify the composition law of four-momenta when pairing two clusters: in our case, $p_{ij}^\mu = p_i^\mu + p_j^\mu$.

¹²The Cambridge algorithm in fact only modifies the clustering procedure of the Durham jet finder and the two implementations coincide for $n \leq 3$ parton final states.

motivation. The D and C ones are different versions of ‘transverse-momentum’ based algorithms, whereas the J and G ones use an ‘invariant-mass’ measure (see [52] for a review). In fact, these two categories are those that have so far been employed most in phenomenological studies of jet physics in electron-positron collisions, with the former gradually overshadowing the latter, thanks to their reduced scale dependence in higher order QCD (e.g., in the case of the $\mathcal{O}(\alpha_s^2)$ three- [52] – [54] and $\mathcal{O}(\alpha_s^3)$ four-jet rates [55]) and to smaller hadronisation effects in the same contexts (see Refs. [52, 53]).

Fig. 4 presents the $A(y)$, $-A_W(y)$ and $B(y)$ coefficients entering eqs. (4.4)–(4.5), as a function of $y(\equiv y_{\text{cut}})$ for the four above jet algorithms at LEP1¹³. Upon multiplying $B(y)$ by $(\frac{\alpha_s}{2\pi})$, a comparison to $A(y)$ and $A_W(y)$ reveals that the NLO-W corrections are negative and remain indeed at the percent level, i.e., of order $\frac{\alpha_{\text{EM}}}{2\pi s_W^2}$ without any logarithmic enhancement (since $\sqrt{s} \approx M_W$). They give rise to corrections to $\sigma_3(y)$ of around 2%, and thus are generally much smaller than the NLO-QCD ones. In this context, no systematic difference is seen with respect to the choice of jet clustering algorithm, over the typical range of application of the latter at LEP1 (say, $y_{\text{cut}} \gtrsim 0.005$ for D, C and $y_{\text{cut}} \gtrsim 0.01$ for G, J).

Table. 1 reports the total three-jet cross-section, i.e., the numerator of the right-hand side of eq. (4.3) for $n = 3$, at LO and the two corrections to it, NLO-QCD and NLO-W, at the representative LEP2 energy of $\sqrt{s} = 200$ GeV. Again, given the relatively small collider energy compared to the EW scale M_W , the pattern already seen at LEP1 for the relative size of the NLO effects is repeated here.

$\sigma_3(e^+e^- \rightarrow \bar{q}qg)$ (pb)			
\sqrt{s} (GeV)	LO	NLO-QCD	NLO-W
200	13.	−3.26	+0.24
D scheme		$y_{\text{cut}} = 0.001$	

Table 1: Total cross-sections for the tree-level process (4.1) alongside the NLO-QCD and NLO-W corrections, at $\sqrt{s} = 200$ GeV, for the D scheme with $y_{\text{cut}} = 0.001$.

Figs. 5 and 6 show the energy dependence of the total cross-section $\sigma_3(y)$ at LO and the corresponding NLO-W correction alongside the relative size of the latter for processes (4.1) and (4.2), respectively, over the energy range $200 \text{ GeV} \leq \sqrt{s} \leq 3 \text{ TeV}$, that is, from LEP2 up to typical CLIC energies [1]. One can appreciate the doubly logarithmic growth with energy of the NLO-W term, whose size increases up to 15–20% of the LO rate at the upper end of the energy spectrum. Indeed, well above 500 GeV, the correction term in Figs. 5 and 6 is substantially reproduced by the expression $\frac{\alpha_{\text{EW}}}{4\pi} \log^2 \frac{s}{M_W^2}$. Furthermore, one may clearly notice at $\sqrt{s} \approx 2m_t$ the threshold effect of the one-loop weak diagrams in which a pair of virtual top quarks is produced in triangle- and box-type graphs. The effect is, as expected, more pronounced for process (4.2) than for process (4.1). Rates are

¹³Notice that $A(y)$ and $A_W(y)$ for the C scheme are identical to those for the D one (recall the previous footnote)

plotted here only for the D scheme with $y_{\text{cut}} = 0.001$, for reference, as the pattern seen for other choices of algorithm and/or resolution parameter is very similar.

Fig. 7 is the counterpart of Fig. 4 for a LC with $\sqrt{s} = 1$ TeV. Since in this case one has that $\sqrt{s} \gg M_W$, the NLO-W corrections are rather large and comparable to the NLO-QCD ones over the interesting y range, hence well above typical experimental uncertainties entering the determination of three-jet observables at LC energies. Besides, contrary to the lower energy case, NLO-W effects are here always positive. At these energies, the NLO-W corrections are of order 10%. Such corrections are likely to be similar in size to the next-to-next-to-leading order (NNLO) corrections from QCD. Indeed, if the speculation in Ref. [45] that the dominant contribution to the QCD correction exponentiates, then at $\sqrt{s} = 1$ TeV, the NNLO-QCD corrections should be in the same range.

In view of this, it is then worthwhile considering the effects of NLO-W corrections to some other ‘infrared-safe’ jet observables typically used in the determination of α_S , the so-called ‘shape variables’ [56]. A representative quantity in this respect is the Thrust (T) distribution [57]. This is defined as the sum of the longitudinal momenta relative to the (Thrust) axis n_T chosen to maximise this sum, i.e.:

$$T = \max \frac{\sum_i |\vec{p}_i \cdot \vec{n}_T|}{\sum_i |\vec{p}_i|}, \quad (4.9)$$

where i runs over all final state clusters. This quantity is identically one at Born level, getting the first non-trivial contribution through $\mathcal{O}(\alpha_S)$ from events of the type (4.1)–(4.2). Also notice that any other higher order contribution will affect this observable. Through $\mathcal{O}(\alpha_S^2)$, for the choice $\mu = \sqrt{s}$ of the renormalisation scale, the T distribution can be parametrised in the following form:

$$(1 - T) \frac{d\sigma}{dT} \frac{1}{\sigma_0} = \left(\frac{\alpha_S}{2\pi}\right) A^T(T) + \left(\frac{\alpha_S}{2\pi}\right)^2 B^T(T). \quad (4.10)$$

Again, the replacement

$$A^T(T) \rightarrow A^T(T) + A_W^T(T) \quad (4.11)$$

accounts for the inclusion of the NLO-W contributions.

We plot the terms $\left(\frac{\alpha_S}{2\pi}\right) A^T(T)$, $\left(\frac{\alpha_S}{2\pi}\right) A_W^T(T)$ and $\left(\frac{\alpha_S}{2\pi}\right)^2 B^T(T)$ in Fig. 8, always at $\sqrt{s} = 1$ TeV, alongside the relative rates of the NLO-QCD and NLO-W terms with respect to the LO contribution. Again, it can be seen that the NLO-W effects can reach the level of +10% or so. We then combine in Fig. 9 the above expressions for the Thrust coefficient functions into the complete event shape distribution, according to eq. (4.10). Here, alongside the LO, NLO-QCD and NLO-W results, we add an estimate of the NNLO-QCD effects based on the considerations of Ref. [45], all plotted over a restricted T range, where experimental fits are usually performed. Here, it can be appreciated that the NLO-W effects are indeed of the same size as those expected from NNLO-QCD. Exact calculations of the latter are currently being performed by several groups [48], [36] – [65].

The ability to polarise electron (and possibly, positron) beams renders future LCs a privileged environment in which to test the differential structure of hadronic samples. In fact, our earlier remark should be recalled: that the latter may well carry the distinctive

hallmark of some new and heavy strongly interactive particles (such as squarks and gluinos in Supersymmetry), whose rest mass is too large for these to be produced in pairs as real states but that may enter as virtual objects into multi-jet events. Similar effects may however also be induced by the NLO-W corrections tackled here. Therefore, as a benchmark for future studies along the above lines, we reproduce in Figs. 10–11 the differential structure of the nine form-factors given in eq. (3.8) for processes (4.1)–(4.2), as a function of the energy fractions x_1 and x_2 , at $\sqrt{s} = 1$ TeV (at this energy, the shape is basically the same for both final states in (4.1)–(4.2)), for the case of a left- and right-handed incoming electrons, respectively. As already intimated in the previous Section, F_7 to F_9 are identically zero at LO¹⁴, even prior to any integration in α, β and/or averaging over the e^+e^- helicities. Besides, F_7 would remain zero unless corrections involve parity-violating interactions. As for F_1, \dots, F_6 , we should mention that the NLO-W corrections to the corresponding tree-level distributions were found of the order 10–15% on average, with some maxima/minima of order 50% in specific regions of the x_1, x_2 plane: e.g., for F_5 when $x_1, x_2 \rightarrow 1$ and for F_6 when $x_1 \rightarrow 0$ and $x_2 \rightarrow 1$, for both the left- and right-handed electron polarisations¹⁵.

Notice that all of the nine distributions in Figs. 10–11, in the presence of a precise determination of α and β (or, for that matter, any other combination of angles used to parametrise the event orientation), are directly observable in the case the $\bar{b}bg$ final state if also the charge (other than the flavour) of the quark is known, e.g., via high- p_T lepton tagging from B -meson decays or via global jet charge determination. If not, all distributions in Figs. 10–11 have to be symmetrised around the $x_1 = x_2$ direction. In the case of the full hadronic sample $\bar{q}qg$, when no flavour tagging is available, one normally identifies the two most energetic jets in the three-jet sample with those originating from the quark-antiquark pair. Although not always true, this approach is known to be a good approximation for most studies (see, e.g., Ref. [66]). Hence, even in this case one may be able to verify to a good approximation the shape of the form-factors F_1, \dots, F_9 in terms of the energy fractions.

Finally, Fig. 12 presents the shape and normalisation of what we call the ‘unintegrated’ (or ‘oriented’) Thrust distributions associated to each of the form-factors in eq. (3.10) (wherein $S = T$), at any fixed values of α and β , alongside the absolute value of the relative size of the NLO-W corrections with respect to the LO case, for the form-factors F_1, \dots, F_6 , which are non-zero at the Born level. Here, the form-factors have been averaged over the electron beam polarisations. For these form-factors NLO-W corrections can be either positive or negative, depending on the form-factor being considered, and can be as large as 10–12% or so.

5. Conclusions

On the basis of our numerical findings in the previous Section, we should like to conclude as follows.

¹⁴This is strictly true only for massless quarks, as, for $m_q \neq 0$, Ref. [41] has shown that F_9 becomes non-zero.

¹⁵For reason of space, we refrain from presenting here the LO dependence of F_1, \dots, F_6 in term of x_1 and x_2 . This can easily be reproduced starting from the formulae in (3.6).

- At LEP1 and LEP2 energies the size of the NLO-W corrections is rather small, of order percent or so, hence confirming that determinations of α_S at such colliders are stable in this respect and that the SM background to parity-violating effects possibly induced by new physics is well under control.
- As the CM energy of the collider grows, NLO-W effects on the inclusive three-jet cross-section become more and more visible, being competitive with the NLO-QCD ones starting from the TeV region (the one that will be explored by future LCs). Indeed, at such high energies, they could be larger than NNLO-QCD effects. Moreover, when $\sqrt{s} \approx 2m_t$, the NLO-W corrections show a characteristic kinematic feature, a threshold effect depleting their contribution to the cross-section locally by up to a factor of four (in the case of $b\bar{b}g$ final states), induced by virtual $t\bar{t}$ production. This peculiar SM effect should not be mistaken for the onset of some new physics phenomena.
- Exclusive observables in three-jet events are also affected by large NLO-W effects at the TeV scale: e.g., the jet fractions and the Thrust distribution. The experimental error expected at LCs in the determination of α_S from such quantities is of the order of percent, so that the inclusion of NLO-W effects in the corresponding theory predictions is then mandatory.
- Since the exploitation of beam polarisation effects will be a key feature of experimental analyses of hadronic events at future LCs, we have presented the full differential structure of three-jet processes in the presence of polarised electrons and positrons, in terms of the energy fractions of the two leading jets and of two angles describing the final state orientation. The cross-sections were parametrised by means of nine independent form-factors, some of which carrying parity-violating effects which are absent in ordinary QCD and that should appropriately be subtracted from hadronic samples in the search for physics beyond the SM.
- All our results were presented for the case of the factorisable NLO-W effects, i.e., for corrections to the initial and final states only. Whereas these should be sufficient to describe adequately the phenomenology of three-jet events at LEP1 and LEP2 energies, at LC energy scales one expects comparable effects due to the non-factorisable corrections, in which weak gauge bosons connect via one-loop diagrams electrons and positrons to quarks and antiquarks. Their computation is currently in progress and we will report on it in due time.

Acknowledgements

EM and DAR are grateful to the CERN Theory Division and SM to the KEK Theory Division for hospitality while part of this work was been carried out. SM and DAR are grateful to John Ellis for illuminating discussions during the early stages of this project. This research is supported in part by a Royal Society Joint Project within the European Science Exchange Programme (Grant No. IES-14468).

References

- [1] K. Abe *et al.*, [The ACFA Linear Collider Working Group], [hep-ph/0109166](#); T. Abe *et al.*, [The American Linear Collider Working Group], [hep-ex/0106055](#); [hep-ex/0106056](#); [hep-ex/0106057](#); [hep-ex/0106058](#); J.A. Aguilar-Saavedra *et al.*, [The ECFA/DESY LC Physics Working Group], [hep-ph/0106315](#); G. Guignard (editor), [The CLIC Study Team], preprint CERN-2000-008 (2000).
- [2] M. Kuroda, G. Moulataka and D. Schildknecht, *Nucl. Phys.* **B 350** (1991) 25;
G. Degrossi and A. Sirlin, *Phys. Rev.* **D 46** (1992) 3104;
A. Denner, S. Dittmaier and R. Schuster, *Nucl. Phys.* **B 452** (1995) 80;
A. Denner, S. Dittmaier and T. Hahn, *Phys. Rev.* **D 56** (1997) 117;
A. Denner and T. Hahn, *Nucl. Phys.* **B 525** (1998) 27.
- [3] W. Beenakker, A. Denner, S. Dittmaier, R. Mertig and T. Sack, *Nucl. Phys.* **B 410** (1993) 245; *Phys. Lett.* **B 317** (1993) 622.
- [4] P. Ciafaloni and D. Comelli, *Phys. Lett.* **B 446** (1999) 278 [[hep-ph/9809321](#)].
- [5] M. Ciafaloni, P. Ciafaloni and D. Comelli, *Phys. Rev. Lett.* **84** (2000) 4810 [[hep-ph/0001142](#)].
- [6] M. Ciafaloni, P. Ciafaloni and D. Comelli, *Phys. Rev. Lett.* **87** (2001) 211802 [[hep-ph/0103315](#)].
- [7] M. Ciafaloni, P. Ciafaloni and D. Comelli, *Nucl. Phys.* **B 613** (2001) 382 [[hep-ph/0103316](#)].
- [8] M. Beccaria, P. Ciafaloni, D. Comelli, F. M. Renard and C. Verzegnassi, *Phys. Rev.* **D 61** (2000) 073005 [[hep-ph/9906319](#)].
- [9] M. Beccaria, P. Ciafaloni, D. Comelli, F. M. Renard and C. Verzegnassi, *Phys. Rev.* **D 61** (2000) 011301 [[hep-ph/9907389](#)].
- [10] M. Beccaria, F. M. Renard and C. Verzegnassi, *Phys. Rev.* **D 63** (2001) 053013 [[hep-ph/0010205](#)].
- [11] M. Beccaria, F. M. Renard and C. Verzegnassi, *Phys. Rev.* **D 63** (2001) 095010 [[hep-ph/0007224](#)].
- [12] M. Beccaria, F. M. Renard and C. Verzegnassi, *Phys. Rev.* **D 64** (2001) 073008 [[hep-ph/0103335](#)].
- [13] A. Denner, talk given at the ‘ International Europhysics Conference on High Energy Physics’, Budapest, Hungary, July 12-18, 2001 [[hep-ph/0110155](#)].
- [14] M. Beccaria, S. Prelovsek, F. M. Renard and C. Verzegnassi, *Phys. Rev.* **D 64** (2001) 053016 [[hep-ph/0104245](#)].
- [15] A. Denner and S. Pozzorini, *Eur. Phys. J.* **C 18** (2001) 461 [[hep-ph/0010201](#)].
- [16] A. Denner and S. Pozzorini, *Eur. Phys. J.* **C 21** (2001) 63 [[hep-ph/0104127](#)].
- [17] S. Pozzorini, *Ph.D. Dissertation*, Universität Zürich (2001).
- [18] E. Accomando, A. Denner and S. Pozzorini, *Phys. Rev.* **D 65** (2002) 073003 [[hep-ph/0110114](#)].
- [19] M. Melles, *Phys. Lett.* **B 495** (2000) 81 [[hep-ph/0006077](#)].
- [20] M. Hori, H. Kawamura and J. Kodaira, *Phys. Lett.* **B 491** (2000) 275 [[hep-ph/0007329](#)].

- [21] W. Beenakker and A. Werthenbach, *Nucl. Phys. Proc. Suppl.* **89** (2000) 88 [hep-ph/0006009].
- [22] W. Beenakker and A. Werthenbach, *Phys. Lett.* **B 489** (2000) 148 [hep-ph/0005316].
- [23] W. Beenakker and A. Werthenbach, *Nucl. Phys.* **B 630** (2002) 3 [hep-ph/0112030].
- [24] V. S. Fadin, L. N. Lipatov, A. D. Martin and M. Melles, *Phys. Rev.* **D 61** (2000) 094002 [hep-ph/9910338].
- [25] P. Ciafaloni and D. Comelli, *Phys. Lett.* **B 476** (2000) 49 [hep-ph/9910278].
- [26] J. H. Kühn, A. A. Penin and V. A. Smirnov, *Eur. Phys. J.* **C 17** (2000) 97 [hep-ph/9912503].
- [27] J. H. Kühn, S. Moch, A. A. Penin and V. A. Smirnov, *Nucl. Phys.* **B 616** (2001) 286 [hep-ph/0106298].
- [28] M. Melles, *Phys. Rev.* **D 63** (2001) 034003 [hep-ph/0004056].
- [29] M. Melles, *Phys. Rev.* **D 64** (2001) 014011 [hep-ph/0012157].
- [30] M. Melles, *Phys. Rev.* **D 64** (2001) 054003 [hep-ph/0102097].
- [31] M. Melles, preprint PSI-PR-01-07 [hep-ph/0104232].
- [32] M. Melles, *Eur. Phys. J.* **C 24** (2002) 193 [hep-ph/0108221].
- [33] J. Layssac and F. M. Renard, *Phys. Rev.* **D 64** (2001) 053018 [hep-ph/0104205].
- [34] See, e.g.:
M. Consoli and W. Hollik (conveners), in proceedings of the workshop ‘Z Physics at LEP1’ (G. Altarelli, R. Kleiss and C. Verzegnassi, eds.), preprint CERN-89-08, 21 September 1989 (and references therein).
- [35] V.A. Khoze, D.J. Miller, S. Moretti and W.J. Stirling, *J. High Energy Phys.* **07** (1999) 014.
- [36] R.K. Ellis, D.A. Ross and A.E. Terrano, *Nucl. Phys.* **B 178** (1981) 421.
- [37] G. Passarino and M.J.G. Veltman, *Nucl. Phys.* **B160** (1979) 151.
- [38] J.A.M. Vermaseren, preprint NIKHEF-00-032 [math-ph/0010025].
- [39] J. Küblbeck, M. Böhm and A. Denner, *Comput. Phys. Commun.* **64** (1991) 165.
- [40] G.J. van Oldenborgh, *Comput. Phys. Commun.* **66** (1991) 1.
- [41] A. Brandenburg, L. Dixon and Y. Shadmi, *Phys. Rev.* **D 53** (1996) 1264 [hep-ph/9505355].
- [42] J.G. Körner and G. Schuler, *Z. Physik* **C 26** (1985) 559; K. Hagiwara, T. Kuruma and Y. Yamada, *Nucl. Phys.* **B 358** (1991) 80.
- [43] A. Ballestrero, E. Maina and S. Moretti, *Phys. Lett.* **B 294** (1992) 425; *Nucl. Phys.* **B 415** (1994) 265 [hep-ph/9212246].
- [44] G. Rodrigo, A. Santamaria and M. Bilenky, *Phys. Rev. Lett.* **79** (1997) 193 [hep-ph/9703358]; *J. Phys.* **G 25** (1999) 1593 [hep-ph/9703360]; preprint FTUV/98-20, IFIC/98-20 [hep-ph/9802359];
G. Rodrigo, preprint ISBN 84-370-2989-9 [hep-ph/9703359]; *Nucl. Phys. Proc. Suppl.* **54 A** (1997) 60 [hep-ph/9609213];
W. Bernreuther, A. Brandenburg and P. Uwer, *Phys. Rev. Lett.* **79** (1997) 189 [hep-ph/9703305];
A. Brandenburg and P. Uwer, *Nucl. Phys.* **B 515** (1998) 279 [hep-ph/9708350];
P. Nason and C. Oleari, *Phys. Lett.* **B 407** (1997) 57 [hep-ph/9705295]; *Nucl. Phys.* **B 521** (1998) 237 [hep-ph/9709360].

- [45] D.A. Ross, *Nucl. Phys.* **B 188** (1981) 109.
- [46] F. Bloch and A. Nordsieck, *Phys. Rev.* **52** (1937) 54.
- [47] T. Kinoshita, *J. Math. Phys.* **3** (1962) 650;
T.D. Lee and M. Nauenberg, *Phys. Rev.* **133** (1964) 1549.
- [48] F.A. Berends, W.T. Giele and H. Kuijf, *Nucl. Phys.* **B 321** (1989) 595; W.T. Giele and E.W.N. Glover, *Phys. Rev.* **D 46** (1992) 1980.
- [49] JADE Collaboration, *Z. Physik* **C 33** (1986) 23;
S. Bethke, *Habilitation thesis*, preprint LBL 50-208 (1987).
- [50] Yu.L. Dokshitzer, contribution cited in the ‘Report of the Hard QCD Working Group’, in Proceedings of the workshop ‘Jet Studies at LEP and HERA’, Durham, December 1990, *J. Phys* **G 17** (1991) 1537;
S. Catani, Yu.L. Dokshitzer, M. Olsson, G. Turnock and B.R. Webber, *Phys. Lett.* **B 269** (1991) 432.
- [51] Yu.L. Dokshitzer, G.D. Leder, S. Moretti and B.R. Webber, *J. High Energy Phys.* **08** (1997) 001.
- [52] S. Moretti, L. Lönnblad and T. Sjöstrand, *J. High Energy Phys.* **08** (1998) 001.
- [53] S. Bethke, Z. Kunszt, D.E. Soper and W.J. Stirling, *Nucl. Phys.* **B 370** (1992) 310; Erratum, preprint [hep-ph/9803267](#).
- [54] M. Bilenky, G. Rodrigo and A. Santamaria, talk given at the IVth International Symposium on Radiative Corrections (RADCOR98), Barcelona, Catalonia, Spain, 8-12 September 1998, preprint FTUV/98-94, IFIC/98-95 [[hep-ph/9812433](#)]; contribution to the XXIX International Conference on High Energy Physics, Vancouver, Canada, July 1998, preprint FTUV/98-79, IFIC/98-80 [[hep-ph/9811465](#)];
M. Bilenky, S. Cabrera, J. Fuster, S. Marti, G. Rodrigo and A. Santamaria, *Phys. Rev.* **D 60** (1999) 114006.
- [55] Z. Nagy and Z. Trócsányi, *Phys. Rev.* **D 57** (1998) 5793; *ibidem* **D 59** (1999) 014020; Erratum, *ibidem* **D 62** (2000) 099902.
- [56] See, e.g.: Z. Kunszt and P. Nason, (conveners), in proceedings of the workshop ‘Z Physics at LEP1’ (G. Altarelli, R. Kleiss and C. Verzegnassi, eds.), preprint CERN-89-08, 21 September 1989 (and references therein).
- [57] E. Fahri, *Phys. Rev. Lett.* **39** (1977) 1587.
- [58] K. Hagiwara and D. Zeppenfeld, *Nucl. Phys.* **B 313** (1989) 560.
- [59] F.A. Berends, W.T. Giele and H. Kuijf, *Nucl. Phys.* **B 321** (1989) 39.
- [60] N.K. Falck, D. Graudenz and G. Kramer, *Nucl. Phys.* **B 328** (1989) 317.
- [61] Z. Bern, L.J. Dixon, D.A. Kosower and S. Weinzierl, *Nucl. Phys.* **B 489** (1997) 3 [[hep-ph/9610370](#)].
- [62] Z. Bern, L.J. Dixon and D.A. Kosower, *Nucl. Phys.* **B 513** (1998) 3 [[hep-ph/9708239](#)].
- [63] E.W.N. Glover and D.J. Miller, *Phys. Lett.* **B 396** (1997) 257 [[hep-ph/9609474](#)].
- [64] J.M. Campbell, E.W.N. Glover and D.J. Miller, *Phys. Lett.* **B 409** (1997) 503 [[hep-ph/9706297](#)].

- [65] L.W. Garland, T. Gehrmann, E.W.N. Glover, A. Koukoutsakis, and E. Remiddi, *Nucl. Phys.* **B 627** (2002) 107 [[hep-ph/0112081](#)]; preprint IPPP/02/28, DCTP/02/56, CERN-TH/2002-122 [[hep-ph/0206067](#)].
- [66] See, e.g.: T. Hebbeker, *Phys. Rep.* **217** (1992) 69 (and references therein).

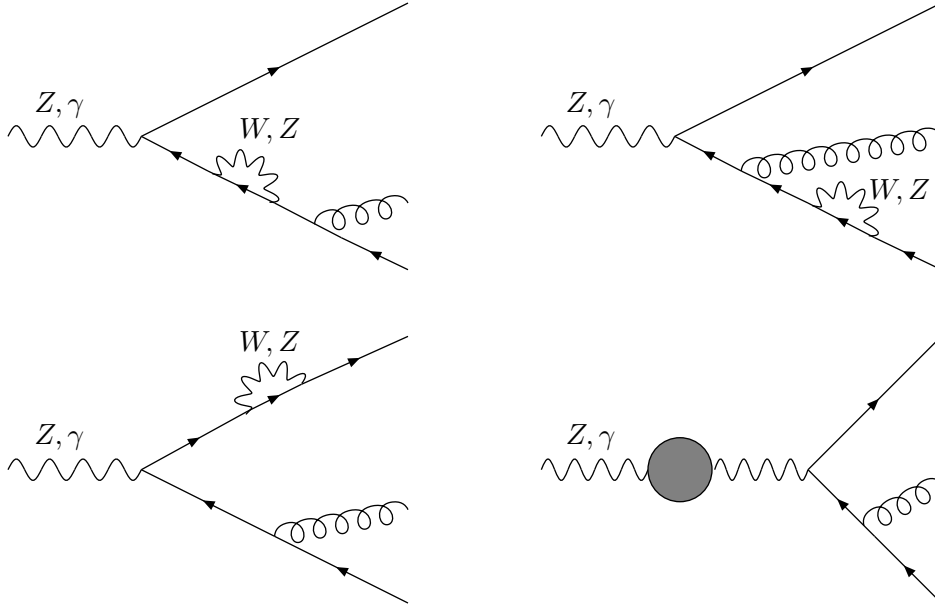


Figure 1: Self-energy insertion graphs. The shaded blob on the incoming wavy line represents all the contributions to the gauge boson self-energy and is dependent on the Higgs mass (hereafter, we will use $M_H = 115$ GeV for the latter). In this and all subsequent figures the graphs in which the exchanged gauge boson is a W -boson is accompanied by corresponding graphs in which the W -boson is replaced by its corresponding Goldstone boson. Since the Yukawa couplings are proportional to the fermion masses, such graphs are only significant in the case of b -quark jets. There is a similar set of diagrams in which the direction of the fermion line is reversed.

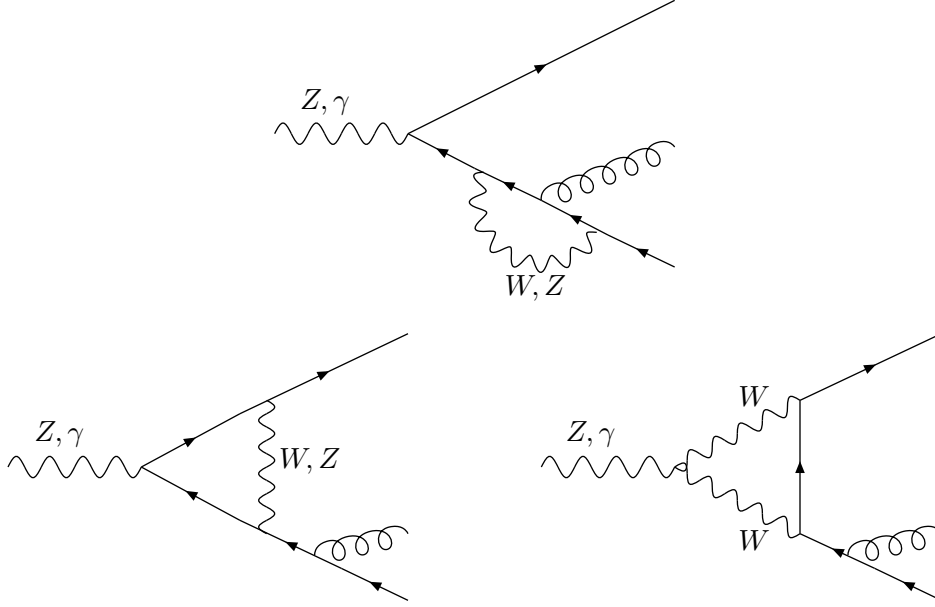


Figure 2: Vertex correction graphs. Again, same considerations as in the previous figure apply for the case of Goldstone bosons and there is a similar set of graphs in which the direction of the fermion line is reversed

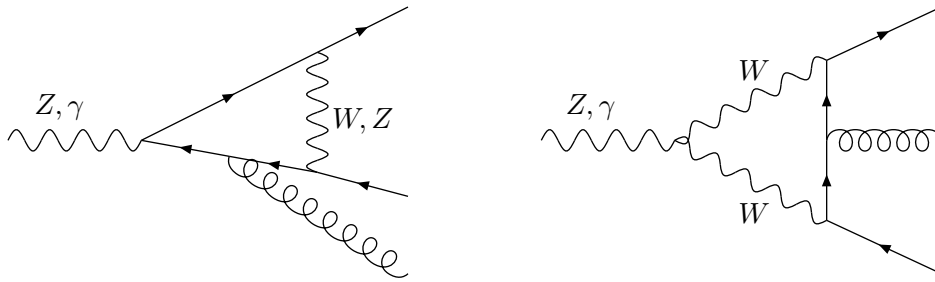


Figure 3: Box graphs. Again, same considerations as in the previous two figures apply for the case of Goldstone bosons. Here, the first graph is accompanied by a similar graph with the direction of the fermion line reversed whereas for the second graph this reversal does not lead to a distinct Feynman diagram.

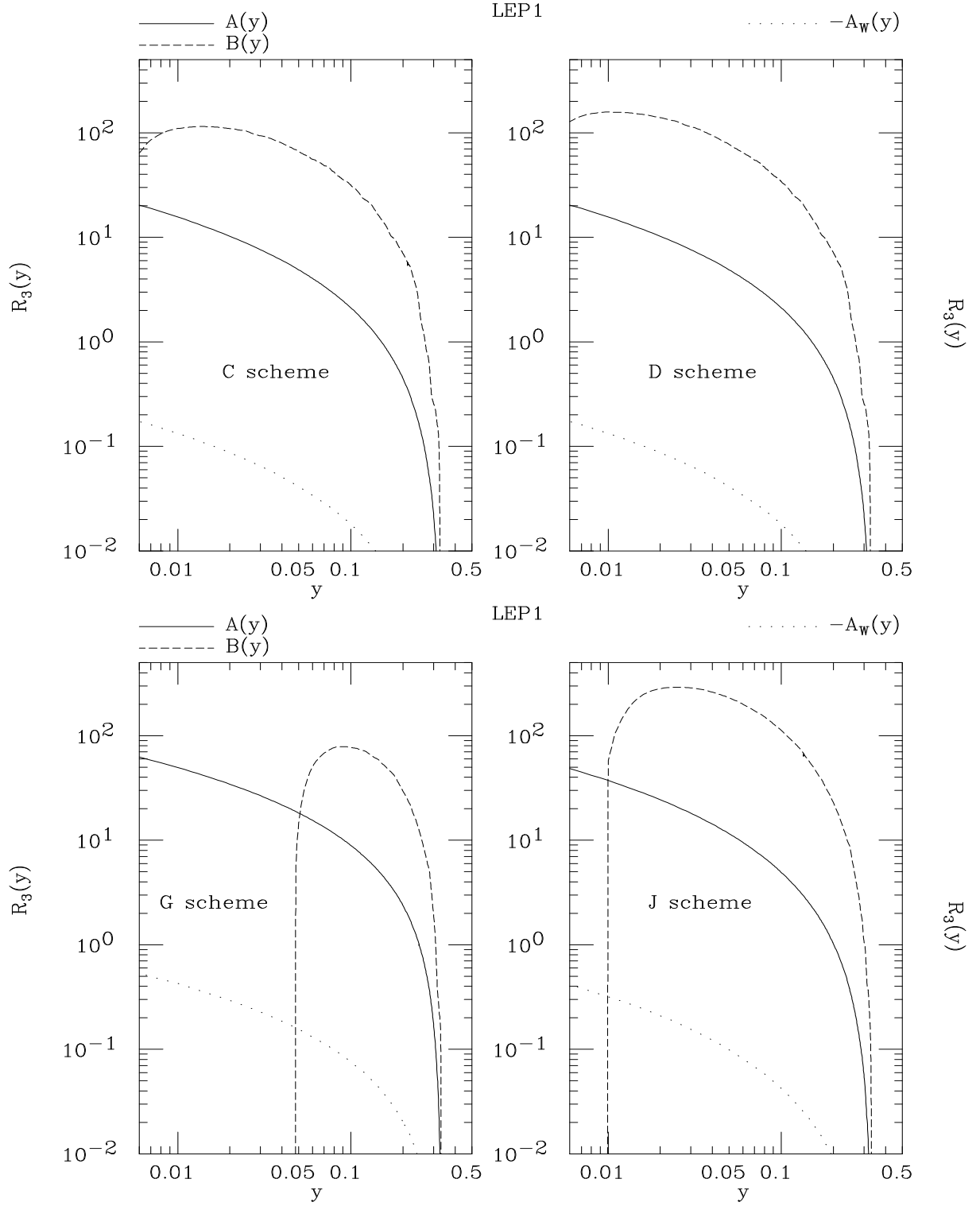


Figure 4: The $A(y)$, $-A_W$ and $B(y)$ coefficient functions of eqs. (4.4)–(4.5) for the Cambridge, Durham, Geneva and Jade jet clustering algorithms, at $\sqrt{s} = M_Z$. (In the plot the sign of A_W has been reversed for better presentation.)

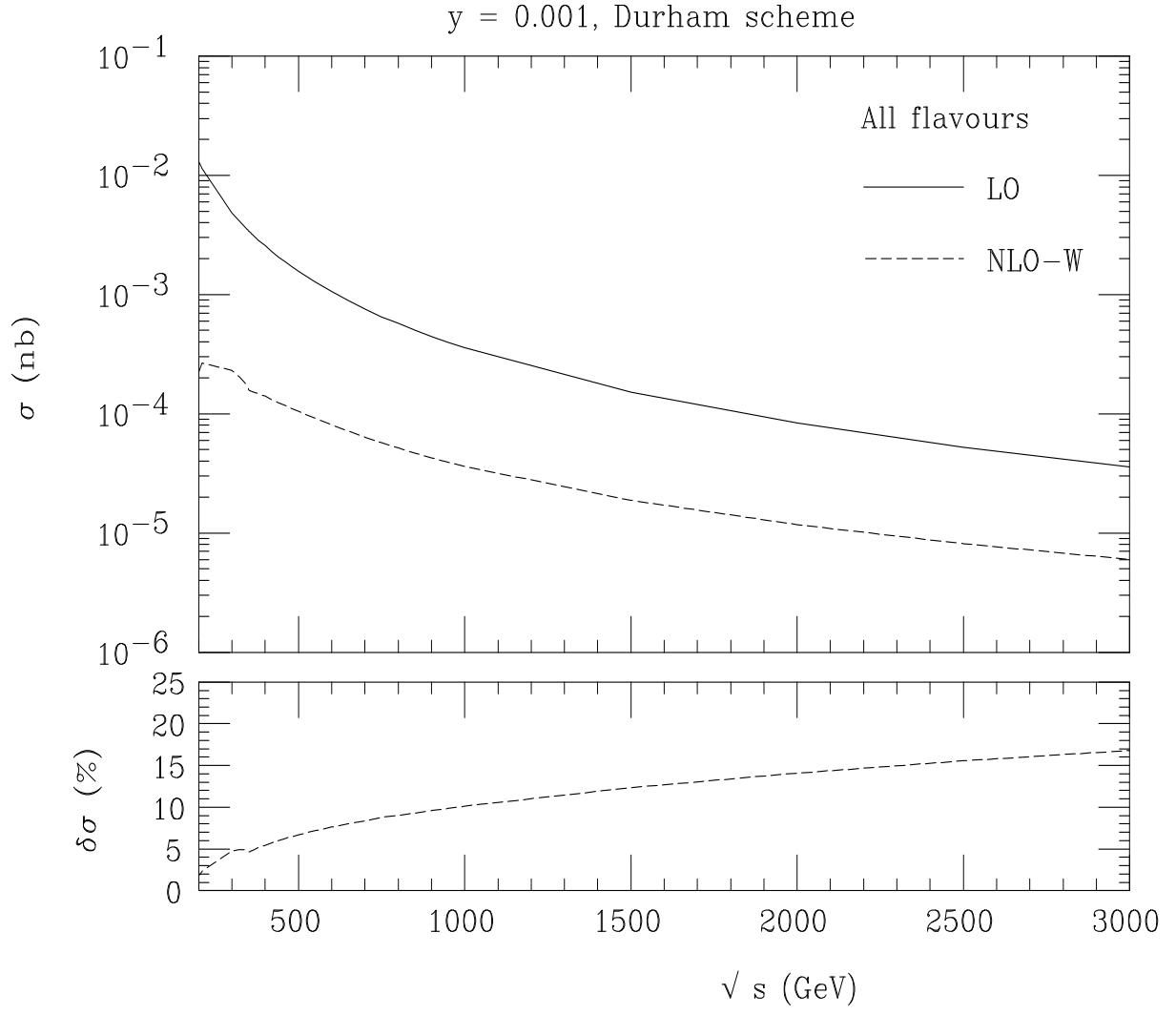


Figure 5: The LO cross-section and NLO-W correction for process (4.1) (top) and the relative size of the latter (bottom) as a function of the collider CM energy.

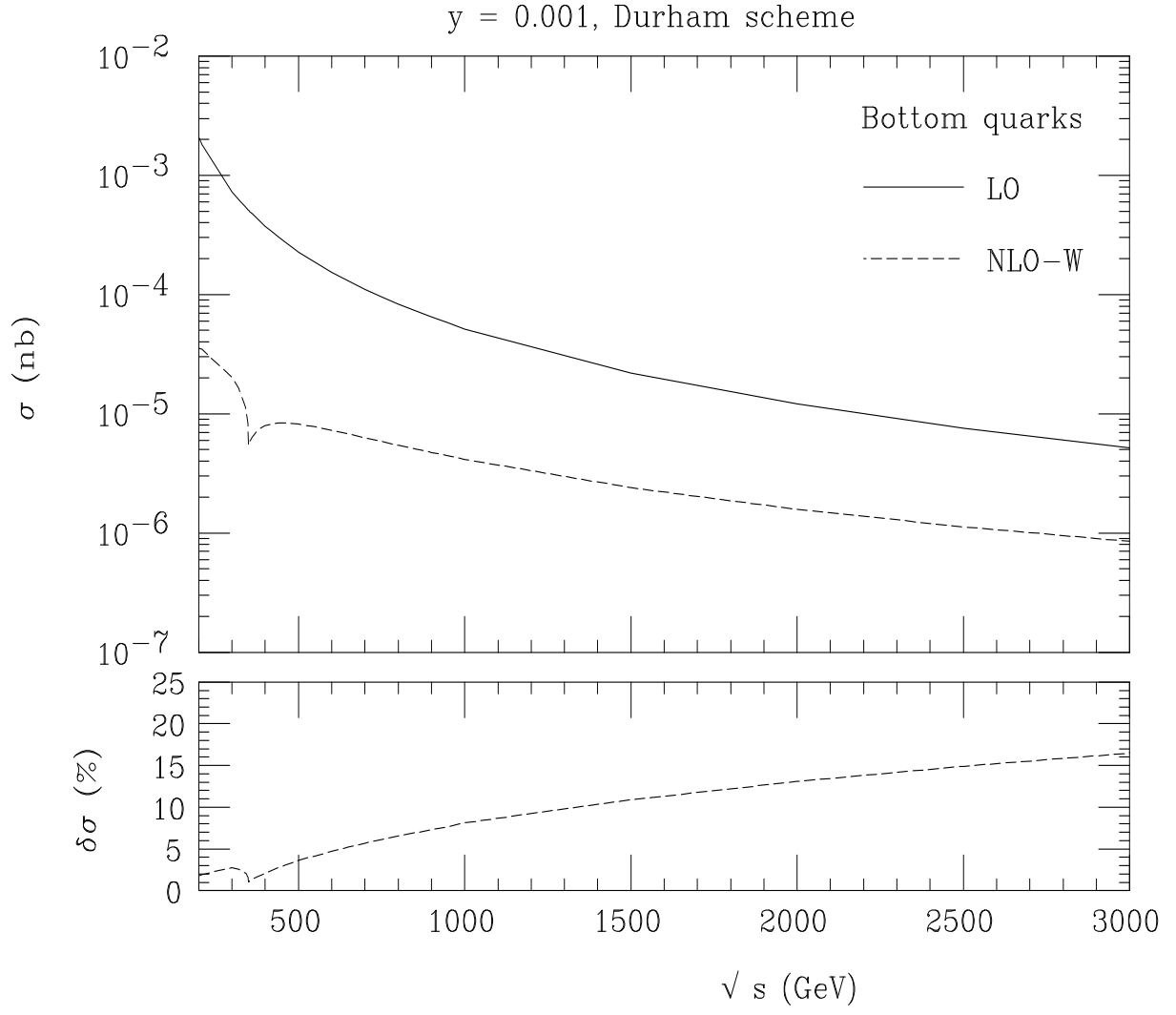


Figure 6: The LO cross-section and NLO-W correction for process (4.2) (top) and the relative size of the latter (bottom) as a function of the collider CM energy.

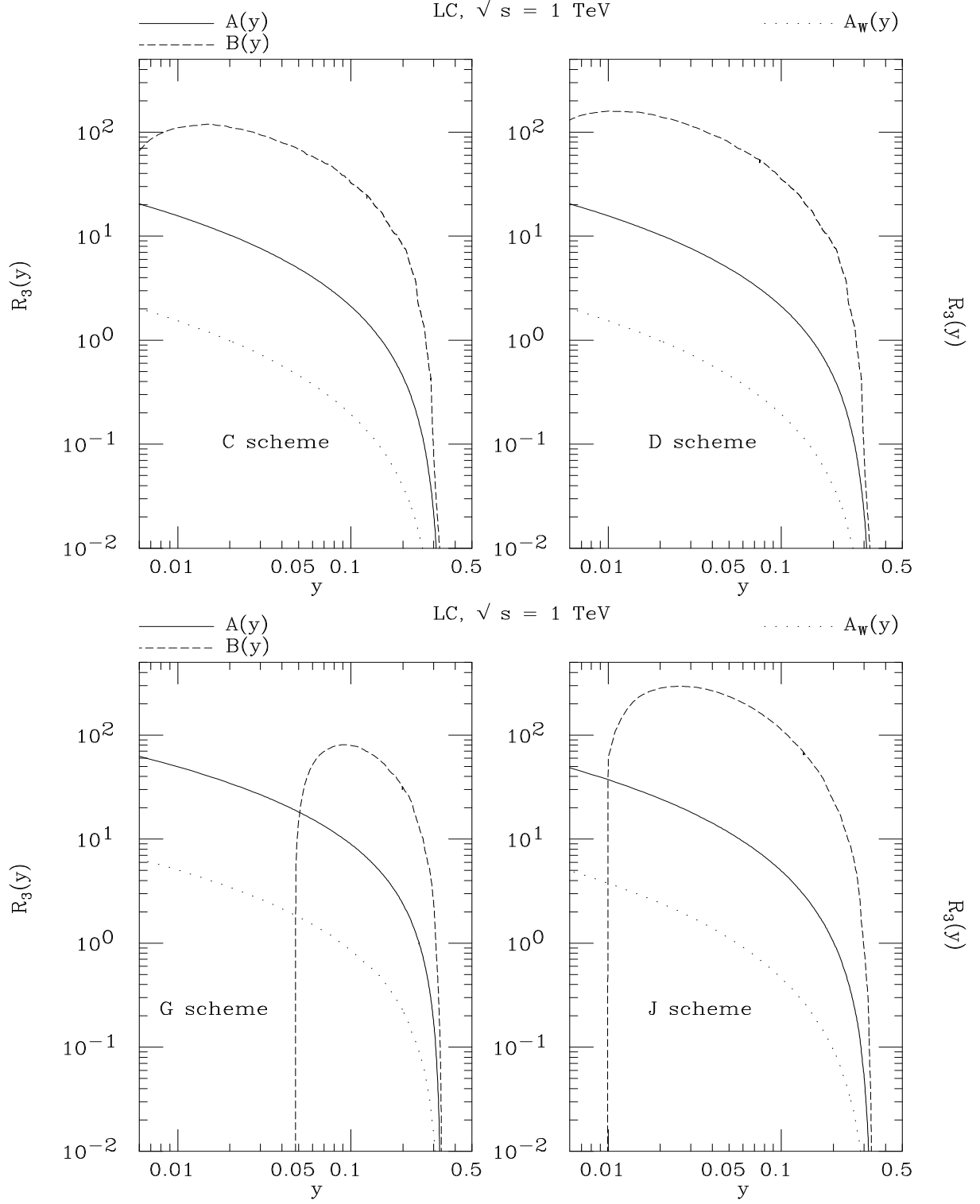


Figure 7: The $A(y)$, A_W and $B(y)$ coefficient functions of eqs. (4.4)–(4.5) for the Cambridge, Durham, Geneva and Jade jet clustering algorithms, at $\sqrt{s} = 1$ TeV.

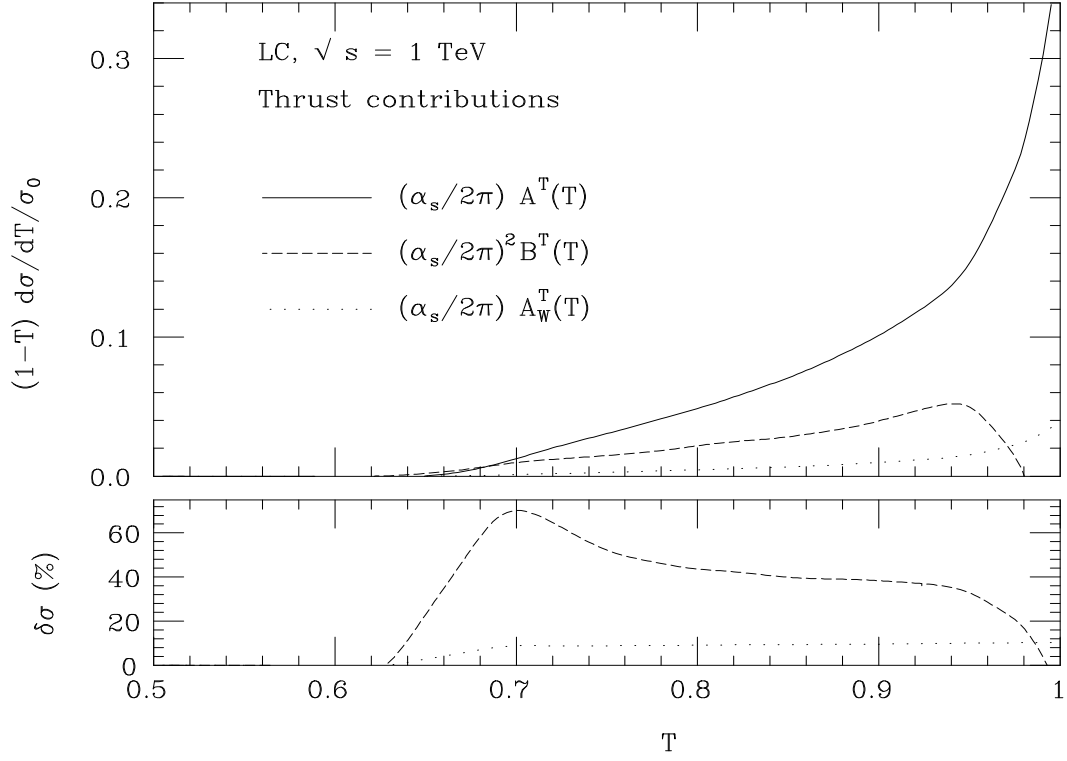


Figure 8: The LO, NLO-QCD and NLO-W contributions to the coefficient functions entering the integrated Thrust distribution, see eq. (4.10), for process (4.1) (top) and the relative size of the two NLO corrections (bottom), at $\sqrt{s} = 1$ TeV.

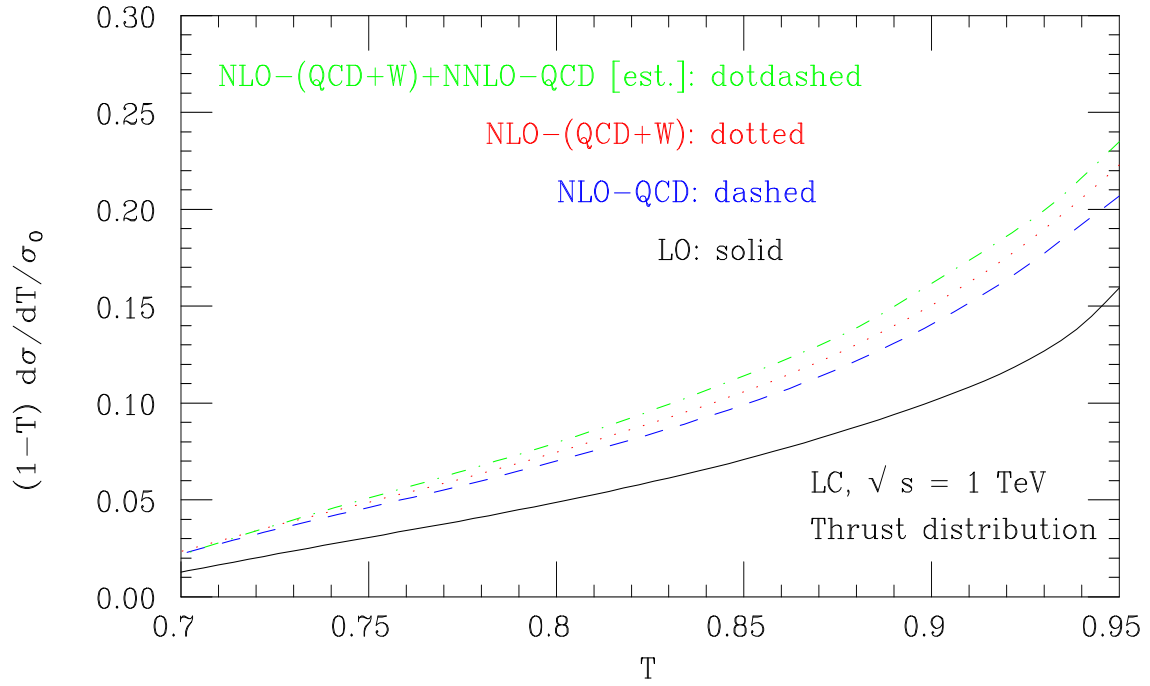


Figure 9: The integrated full Thrust distribution, see eq. (4.10) for process (4.1), at $\sqrt{s} = 1$ TeV. We show separately the LO result and the additional contributions from the exact NLO-QCD, an estimate of the NNLO-QCD and the exact NLO-W corrections, respectively.

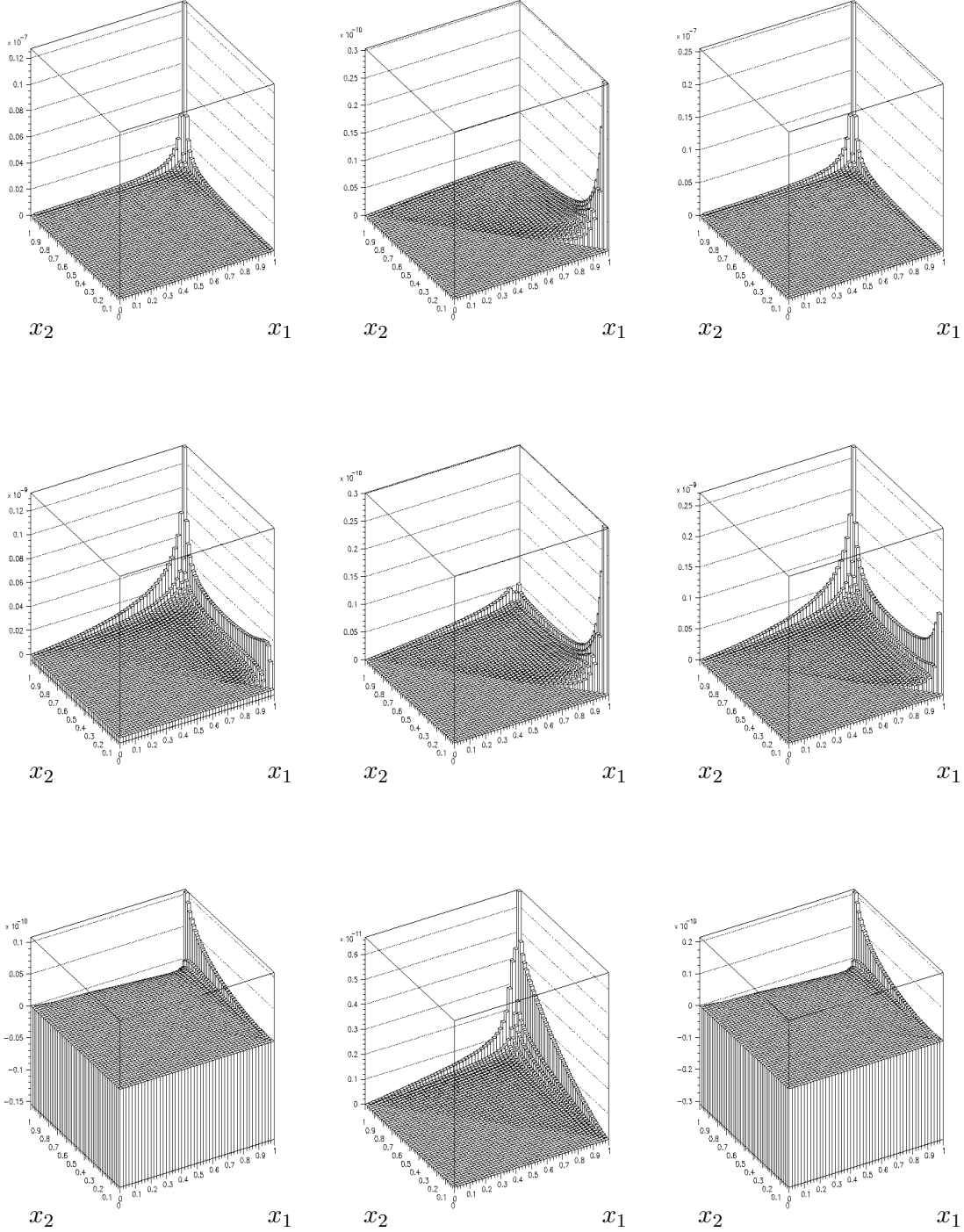


Figure 10: The nine form-factors defined in eq. (3.8) as a function of the antiquark ($i = 1$) and quark ($i = 2$) energy fractions $x_i = \frac{2E_i}{\sqrt{s}}$ at $\sqrt{s} = 1$ TeV in units of nb, for left-handed incoming electrons. (Note that in some cases we plot the opposite of the form-factor.)

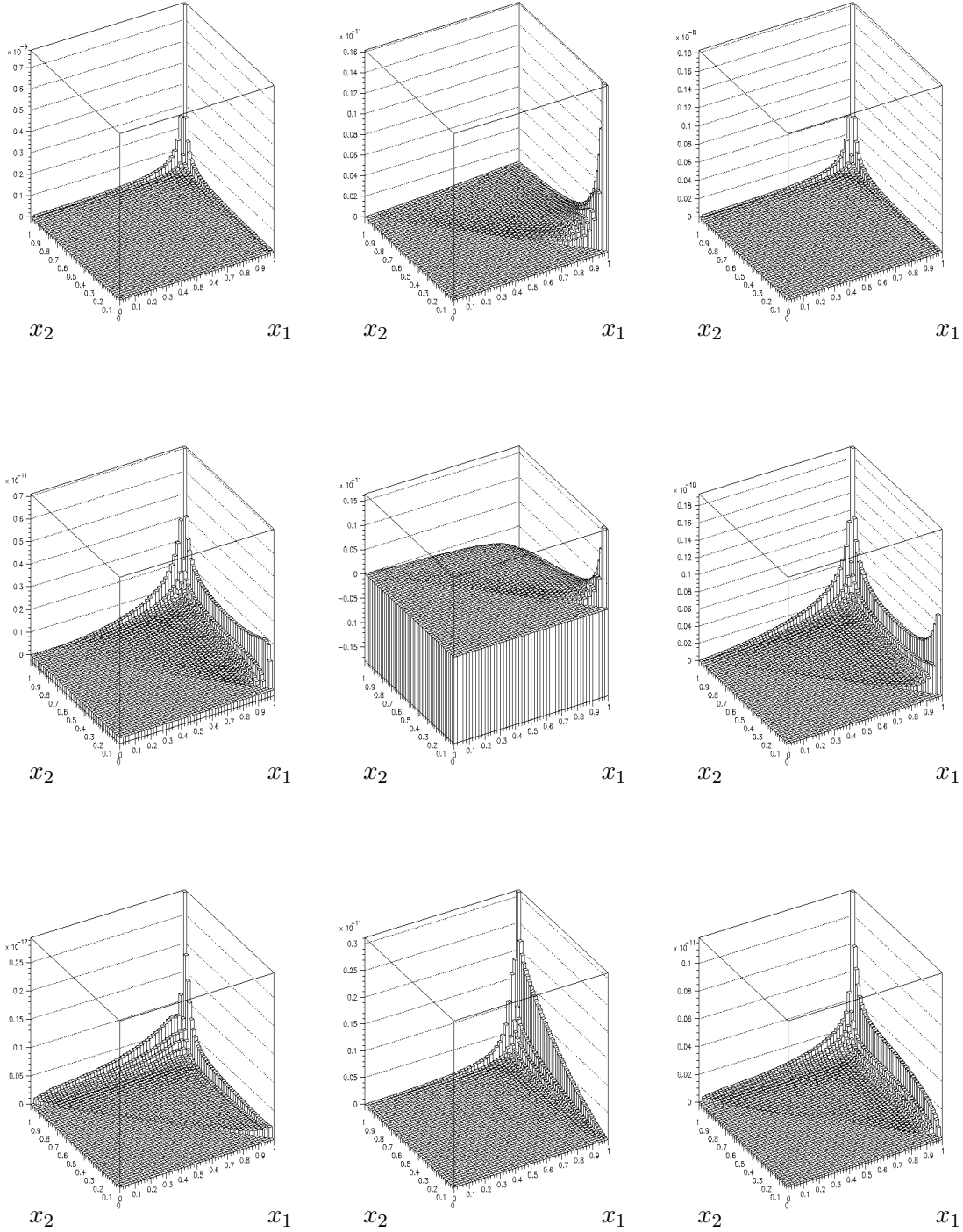


Figure 11: The nine form-factors defined in eq. (3.8) as a function of the antiquark ($i = 1$) and quark ($i = 2$) energy fractions $x_i = \frac{2E_i}{\sqrt{s}}$ at $\sqrt{s} = 1$ TeV in units of nb, for right-handed incoming electrons. (Note that in some cases we plot the opposite of the form-factor.)

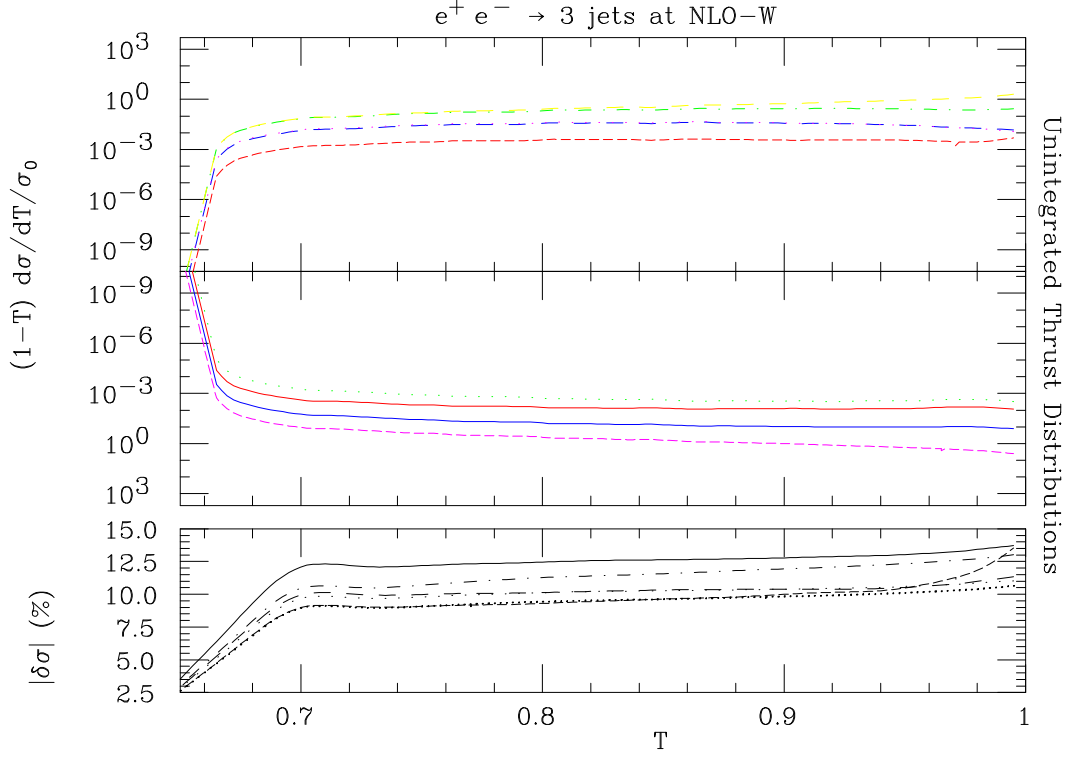


Figure 12: The unintegrated Thrust distributions for the nine component of the cross-section associated to the form-factors in eq. (3.8) for the NLO-W process (4.1) (top and middle) and the relative size of the six components which are non-zero at LO (bottom), at $\sqrt{s} = 1$ TeV. Labels are as follows: (top) F_1 (yellow), F_2 (magenta), F_5 (blue), F_6 (green), F_8 (red); (middle) F_3 (magenta), F_4 (blue), F_7 (green), F_9 (red); (bottom) F_1 (fine-dotted), F_2 (dashed), F_3 (dot-dashed), F_4 (dotted), F_5 (fine-dashed), F_6 (solid).